Numerical Simulation of Premixed Turbulent Methane Combustion

J. B. Bell, M. S. Day, A. S. Almgren, R. K. Cheng and I. G. Shepherd

Lawrence Berkeley National Laboratory
Berkeley, California, 94720, USA

Abstract. In this paper we study turbulent premixed methane flames with swirl using three-dimensional numerical simulation. The simulations are performed using an adaptive time-dependent low Mach number combustion algorithm based on a second-order projection formulation that conserves both species mass and total enthalpy. The species and enthalpy equations are treated using an operator-split approach that incorporates specialized integration techniques for modeling chemical kinetics. In the present study a simplified two-step reaction mechanism with six species is used. We present computational results for a low swirl burner that stabilizes a freely propagating premixed flame.

1. Introduction

Turbulent premixed combustion is one of the major active research topics in combustion science. A number of computational studies have used detailed simulations of strained flames in one dimension and vortex/flame interactions in two dimensions to study the fluid effects on flame chemistry. There is also an extensive literature describing the development of modeling techniques suitable for large-scale engineering simulations; see, for example, the Proceedings of the Combustion Institute [1]. The recent book by Peters [2] provides an good introduction to turbulent combustion and also contains an excellent bibliography.

In recent years a number of studies were aimed at elucidating key mechanisms in premixed turbulent combustion using direct three-dimensional numerical simulation. Most studies of this type consider the interaction of a laminar flame with decaying isotropic turbulence. Early studies of this type using single step chemistry were performed by Trouve and Poinsot [3], and by Zhang and Rutland [4]. More recently, Tanahashi et al. [5, 6] have performed direct numerical simulations of turbulent, premixed hydrogen flames in three dimensions with detailed hydrogen chemistry. Bell et al. [7] have performed similar

computations for a methane flame with detailed chemistry. Thevenin et al. [8] and Jenkins and Cant [9] have treated the ignition of a methane flame kernel in three dimensions using a modified ILDM treatment of methane chemistry.

In this paper, we discuss simulation of premixed turbulent methane combustion in a laboratory scale burner. The burner configuration we consider uses a grid to generate turbulence in the inflow field and tangential air jets to introduce sufficent swirl to stabilize the flame. We use adaptive mesh refinement to resolve the incoming turbulent field and the flame so that we do not need to introduce subgrid-scale models for turbulence or turbulent chemistry interaction. For the computations presented here we use a simplified two-step kinetics mechanism and focus our analysis on basic flame geometry.

2. Numerical Model

Our computational approach uses a hierarchical adaptive mesh refinement (AMR) algorithm based on an approximate projection formulation for incompressible flow by Almgren et al. [10], subsequently extended to low Mach number combustion by Pember et al. [11]. The methodology was extended to model detailed kinetics and differential diffusion by Day and Bell [12]. The reader is referred to [12] for details of the model and its numerical implementation and to [7] for the application of this methodology to the simulation of premixed turbulent flames.

We consider a gaseous mixture, ignoring Soret and Dufour effects, body forces and radiative heat transfer, and assume a mixture model for species diffusion. The single-grid scheme that forms the basis for our adaptive algorithm combines a symmetric operator-split coupling of chemistry and diffusion processes with a projection method for incorporating the velocity divergence constraint arising from the low Mach number formulation. First, conservation equations are advanced in time for momentum, species density and enthalpy using a second-order Godunov scheme for advective terms and a time-centered Crank-Nicolson discretization for diffusion. Because the transport coefficients depend on both temperature and composition, we adopt a sequential, predictor-corrector scheme to guarantee second-order treatment of nonlinear diffusion effects. The chemistry is advanced using CHEMEQ2, a solver for stiff ODEs arising from reaction kinetics [13]. The implicit diffusion and chemistry components of the algorithm are time-split symmetrically to ensure that the composite algorithm remains second-order accurate. The velocity field resulting from the advection/diffusion/chemistry step is then decomposed using a density-weighted approximate projection. The component satisfying the elliptic constraint updates the velocity field, and the remainder updates the perturbational pressure.

The extension of the above algorithm to AMR is based on a hierarchical refinement strategy using a system of overlaid grids. Fine cells are formed by uniformly dividing

coarse cells in all three directions; fine grid patches are rectangular groupings of the fine cells. Increasingly finer levels, each consisting of a union of rectangular grid patches, overlay coarser grid levels until the solution is adequately resolved. The fine grids are advanced in a subcycled fashion using a CFL-based time step appropriate to that level. Sychronization operations ensure appropriate coupling and conservation across refinement levels. An error estimation procedure identifies where refinement is needed and grid generation procedures dynamically create or remove rectangular fine grid patches as requirements change. The complete adaptive algorithm is second-order accurate in space and time, and discretely conserves species mass and enthalpy. Implementation of this methodology for distributed memory parallel processors is discussed by Bell et al. [14].

3. Burner configuration

The configuration we consider is a modified version of low swirl burners first studied by Bedat and Cheng [15] and Cheng [16] depicted in Fig. 1. The experimental burner nozzle is 50 mm in diameter. Turbulence is generated by a grid located in the nozzle that generates statistically uniform, isotropic turbulence with an integral scale of 5mm and a turblent intensity, u', of 0.18 m/s. Swirl is introduced by four air jets spaced uniformly around the circumference of nozzle that introduce a tangential flow just above the turbulence grid. For this configuration, the intensity of the swirl is defined by a swirl number, S

$$S = \frac{\int_0^R uwr^2 dr}{R \int_0^R u^2 r dr}$$

where u is the normal velocity component and w is the tangential velocity component.

For the computations presented here, we do not attempt to compute the flow within the nozzle. Instead we impose flow conditions at the nozzle exit that are specified from experimental characterization of the flow. Mean profiles of the inflow normal and tangential velocity profiles are depicted in Fig. 2. The fuel mixture is a lean methane-air mixture with equivalence ratio $\phi = 0.6$ for which the laminar flame speed is approximately 0.15 m/sec. The swirl number, $S \approx 2.4$. The use of air jets to introduce swirl leads to dilution of the fuel air mixture near the circumference of the burner. In Fig. 2, we also present the equivalence ratio of the inflow gases as a function of radius.

4. Results

The computational domain is a cube which is 0.20 m on each side with the nozzle exit centered on the lower face. The burner is modeled using the flow profiles described above. In addition, we specify a weak coflow of 0.03 m/sec at the bottom of the computational domain outside the nozzle. The sides of the domain are slip walls and the top is outflow.

At the nozzle inflow we add homogeneous isotropic turbulence to the mean flow profiles. The fluctuations are shaped with a top-hat function to rapidly decrease the intensity to zero at the edge of the nozzle. The turbulence field used in the computation is generated in a separate computation by first computing a synthetic field with spectrum

$$C(k^4/k_o^5)exp(-2*(k/k_o)^2).$$

The parameter, k_o, is chosen to give the appropriate integral scale. This initial field is evolved for several eddy turnover times to guarantee appropriate phasing of the resulting velocities, then scaled to match the turbulent intensity measured in the experiment.

We use a simplified 2-step chemical mechanism for methane combustion developed by Zimont and Trushin [17]. We initialize the computational domain with a laminar flame for this mechanism computed using PREMIX [18] in the region of the domain above the nozzle exit with the flame location near the inflow face. We then allow the system to evolve until the turbulent flame that forms appears to be statistically stationary.

A typical profile of the CO mole fraction is depicted in Fig. 3. The computation is performed using adaptive mesh refinement with a base grid of 128^3. Additional refinement levels are used to ensure adequate resolution of the inflow turbulence and the flame. The narrow region of peaked CO concentration signifies the location of the flame at this instant and fluctuates in time. In a time-averaged sense, the flame surface has increased to accommodate the corresponding increase in fuel rate over the laminar burning velocity. The shape of the flame surface is affected strongly by the mean flow field and turbulent fluctuations.

5. Conclusions

We have applied an existing low Mach number model to the study of a time-dependent three-dimensional turbulent premixed methane flame. The configuration corresponds to an experimental low-swirl burner that uses tagential air jets within the fuel tube to produce an axial velocity deficit in the flow just leaving the fuel jet. In the experiment, the turbulent diverging flow allows a fluctuating, but stable, premixed methane flame just above the nozzle. The simulations presented demonstrate that we can produce a similarly stable flame with our computational methodology. We plan to continue exploring the parameters that affect the mean flow distribution, a range of fuel equivalence ratios, and the effects of various levels of chemical mechanism fidelity on methane combustion.

Acknowledgments

[1] Troe, J. and Williams, F. A., editors, *Proceedings of the Combustion Institute*, Volume 29, The Combustion Institute, Pittsburgh, PA, 2002.

[2] Peters, N., *Turbulent combustion*, Cambridge University Press, 2000.

[3] Trouve, A. and Poinsot, T., *J. Fluid Mech.*, 278:1–31 (1994).

[4] Zhang, S. and Rutland, C. J., *Combust. Flame*, 102:447–461 (1995).

[5] Tanahasi, M., Fujimura, M., and Miyauchi, T., *Proc. Combust. Inst.*, 28:529–535 (2000).

[6] Tanahasi, M., Nada, Y., Ito, Y., and Miyauchi, T., *Proc. Combust. Inst.*, 29 (2002).

[7] Bell, J. B., , Day, M. S., and Grcar, J. F., *Proc. Combust. Inst.*, 29 (2002).

[8] Thevenin, D., Gicquel, O., Charentenay, J. de, Hilbert, R., and Veynante, D, *Proc. Combust. Inst.*, 29 (2002).

[9] Jenkins, K. W. and Cant, R. S., *Proc. Combust. Inst.*, 29 (2002).

[10] Almgren, A. S., Bell, J. B., Colella, P., Howell, L. H., and Welcome, M., *J. Comput. Phys.*, 142:1–46 (1998).

[11] Pember, R. B., Howell, L. H., Bell, J. B., Colella, P., Crutchfield, W. Y., Fiveland, W. A., and Jessee, J. P., *Comb. Sci. Technol.*, 140:123–168 (1998).

[12] Day, M. S. and Bell, J. B., *Combust. Theory Modelling*, 4(4):535–556 (2000).

[13] Mott, D. R. and Oran, E. S., "CHEMEQ2: a solver for the stiff ordinary differential equations of chemical kinetics," NRL Report No. NRL/MR/6400–01-8553.

[14] Bell, J. B., Day, M. S., Almgren, A. S., Lijewski, M. J., and Rendleman, C. A., *Numerical Methods for Fluid Dynamics VII*, ICFD, pp. 207–213March (2001), *also to appear in Int. J. Num. Meth. Fluids.*

[15] Bedat, B. and Cheng, R. K., *Combustion and Flame*, 100:485–494 (1995).

[16] Cheng, R. K., *Combustion and Flame*, 101:1–14 (1995).

[17] Zimont, V. L. and Trushin, Y. M., *Comb. Expl. Shock Wav.*, 5:391–394 (1969).

[18] Kee, R. J., Dixon-Lewis, G., Warnatz, J., Coltrin, M. E., and Miler, J. A., "A FORTRAN computer code package for the evaluation of gas-phase multicomponent transport properties," Sandia Technical Report No. SAND86-8246.

List of Figures
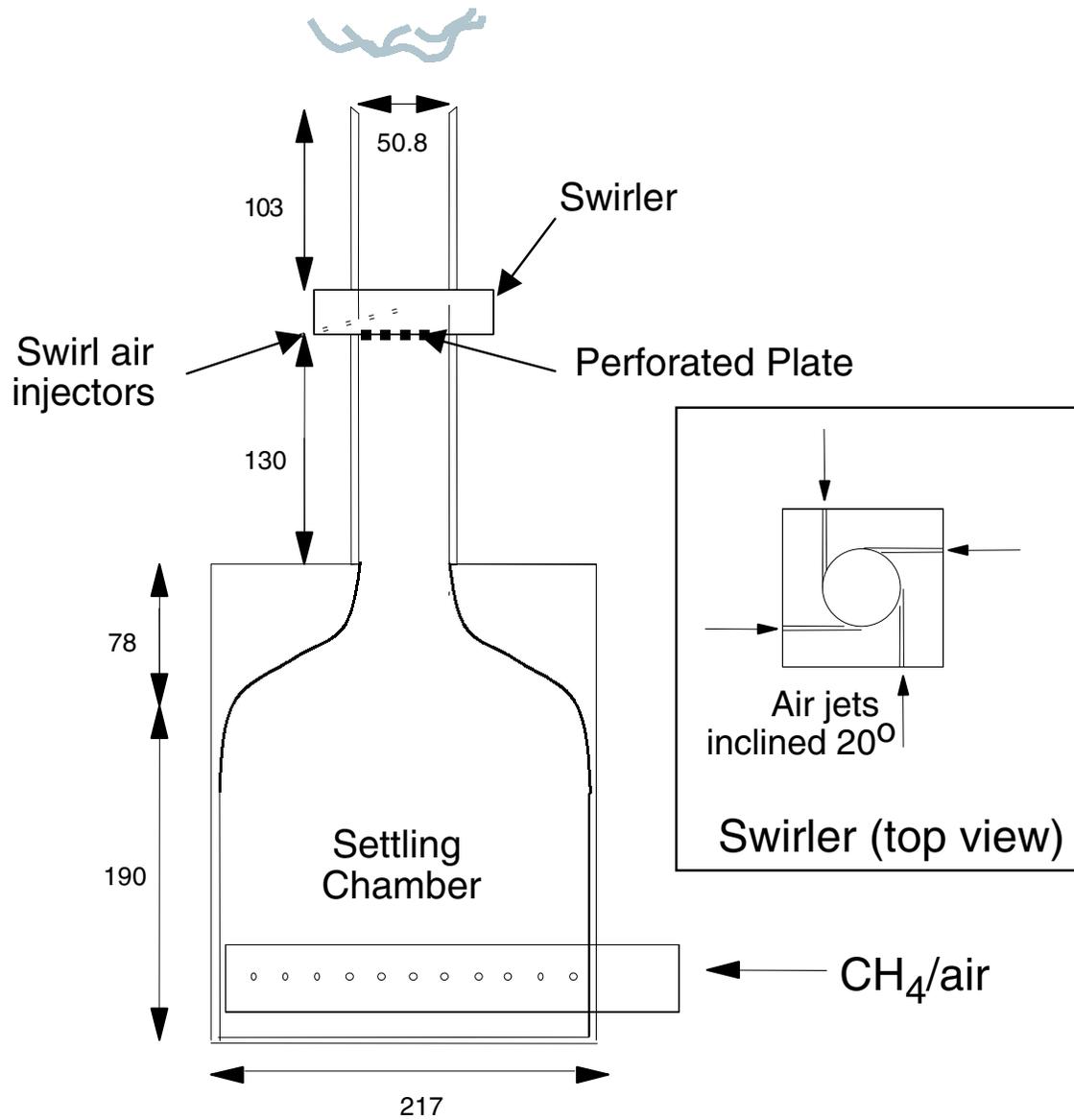
Figure 1. Schematic of the burner configuration used for the simulations
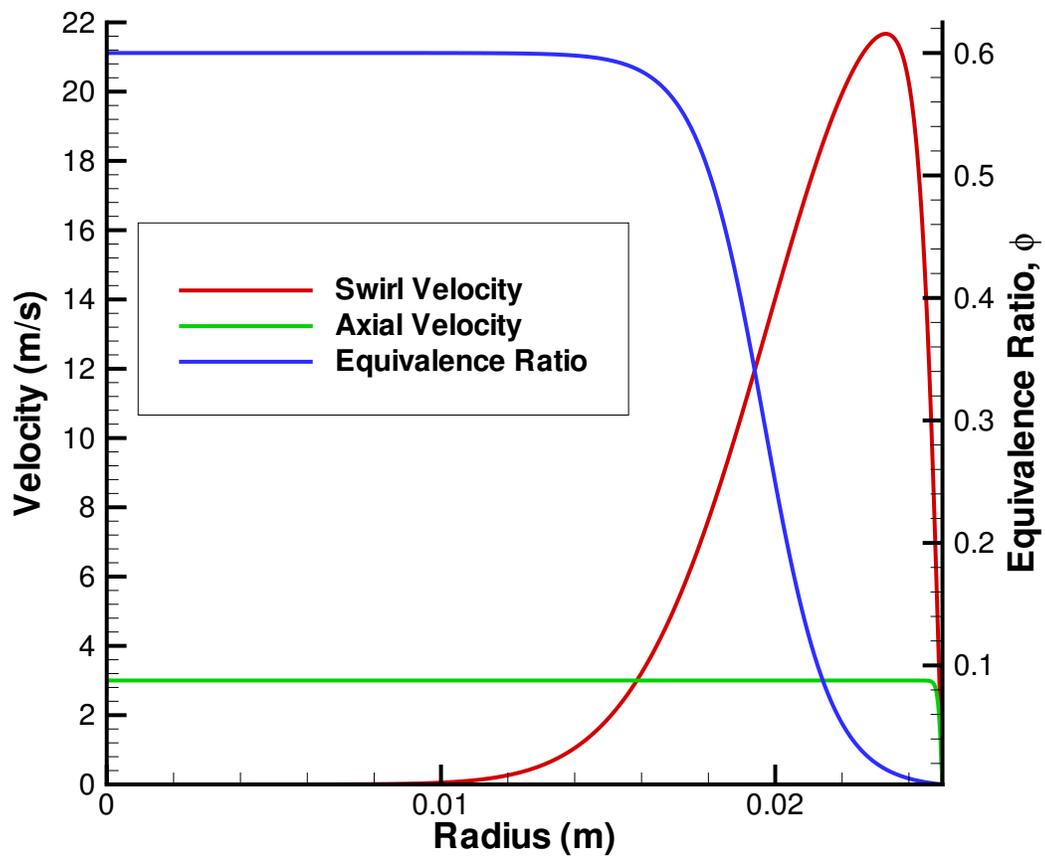
Figure 2. Profiles of normal and tangential velocity and equivalence ratio at the burner exit
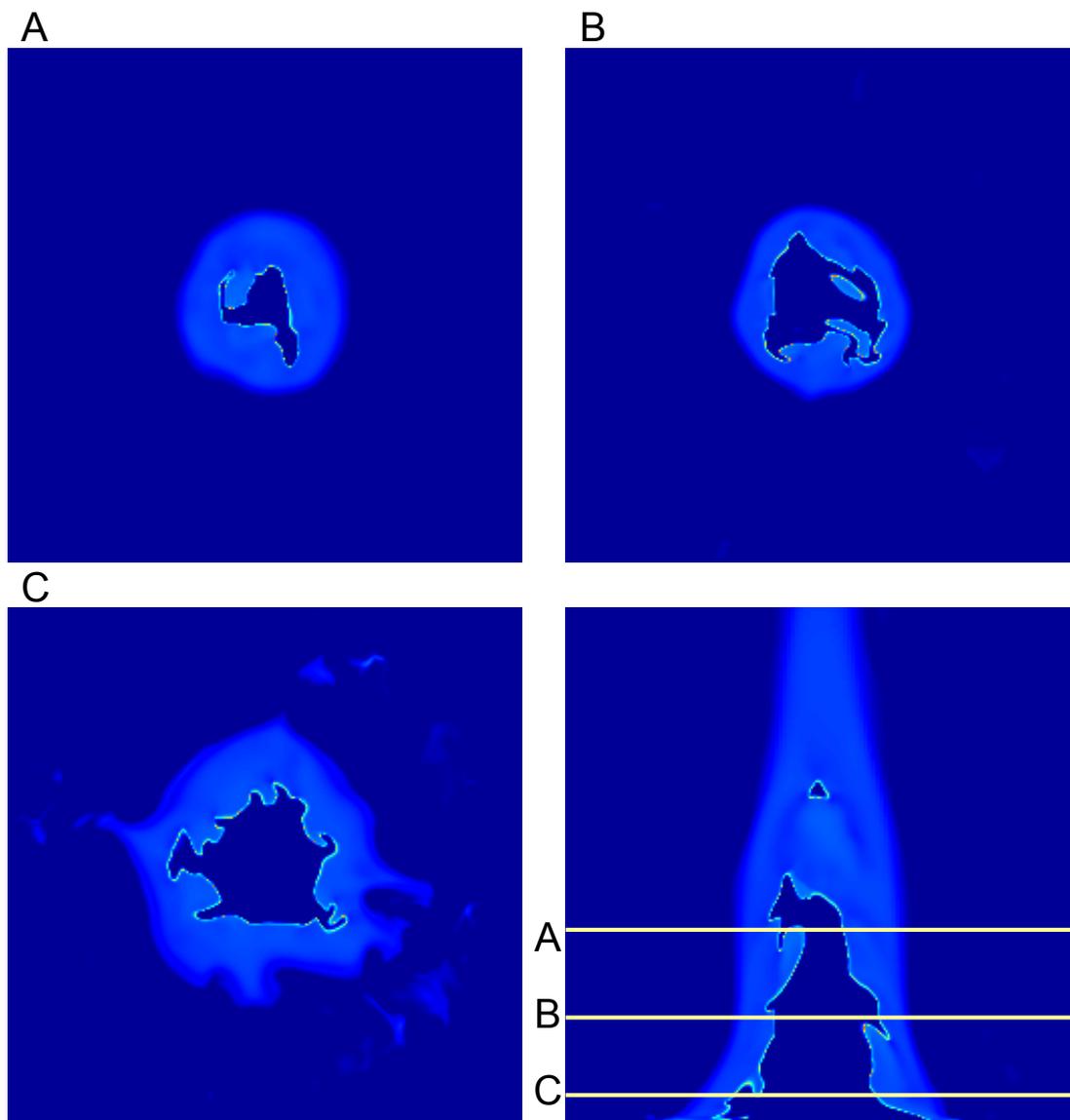
Figure 3. Raster images of the CO mole fraction over the computational domain. The lower right image is a vertical slice through the center of the domain. The three labelled images correspond to horizontal slices taken at the corresponding labelled locations in the vertical slice.